Chemistry and physical properties of axinites

GREGORY R. LUMPKIN AND PAUL H. RIBBE

Department of Geological Sciences, Virginia Polytechnic Institute and State University
Blacksburg, Virginia 24061

Abstract

Electron microprobe analyses of 37 axinites from 31 localities substantiate the conclusions of Kurshakova (1968, 1976) and Sanero and Gottardi (1968) as to the substitutional solid solution among octahedrally-coordinated divalent cations Ca, Mn, Fe, Mg, and Zn. All compositions plot near either of two lines on a triangular diagram with vertices 3Ca–3Mn–3(Fe+Mg+Zn): $2Ca \cdot 1(Fe+Mg) \leftrightarrow 2Ca \cdot 1Mn$ or $2Ca \cdot 1Mn \leftrightarrow 1Ca \cdot 2Mn$, with some Zn substituting for Mn in the latter. The substitution $Al^{3+} + O^{2-} \rightleftharpoons M^{2+} + OH^-$ was observed by Cassedanne *et al.* (1977), and our analyses also suggest possible substitutions of Fe^{3+} for Al in the $AlO_5(OH)$ octahedra and of Al for Si in the $B_2Si_8O_{30}$ groups. The chemistry of the axinite group is best described by a new structural formula:

$$[(Mn,Fe^{2+},Mg,Zn,Al_w)(Ca_{2-x}Mn_x)(Al_{2-y}Fe_y^{3+})]_2^{VI}(OH_{2-w},O_w)[(B_2Si_{8-z}Al_z)^{IV}O_{30}]$$

where $w < 1$, $x < 1$, $y \ll 1$, $z \ll 1$, and VI and IV represent coordination of the cations.

Octahedral and tetrahedral layering approximately parallel to $(\bar{1}11)$, bands of elongate $B_2Si_8O_{30}$ groups parallel to $[0\bar{1}1]$, and four types of octahedral chains influence the orientation of the biaxial indicatrix, the crystal morphology, and the (100) cleavage whose trace is parallel to $[0\bar{1}1]$, requiring the breaking of no bonds within the tetrahedral groups and only (Ca,Al)–(OH,O) and (Fe,Mn,Mg)–O bonds in the octahedral layer. Due to their proximity to octahedral chains, the b and c cell edges have high correlations with the mean radii of octahedral cations. Density and mean refractive index ⟨R.I.⟩ are highly correlated with the transition-metal content in all axinites, and $2V\alpha$ is highly correlated with Mg content for the non-zincian 2Ca-axinites. Reasonable estimates of composition can be obtained for the non-zincian 2Ca-axinites by using the following equations for the mole fraction of Mg, Fe, and Mn:

$$Mg = -14.333⟨R.I.⟩ + 0.012(2V\alpha) + 23.487 \quad (R^2 = 0.997)$$
$$Fe = 71.937⟨R.I.⟩ - 11.810(\rho_{obs}) - 81.890 \quad (R^2 = 0.894)$$
$$Mn = -42.903⟨R.I.⟩ + 12.523(\rho_{obs}) + 31.473 \quad (R^2 = 0.910)$$

Introduction

The axinite group of borosilicates, $[(Mn,Fe^{2+}, Mg,Zn)(Ca,Mn)_2(Al,Fe^{3+})_2]_2(OH)_2[B_2Si_8O_{30}]$, occurs in numerous localities including skarns, pegmatites, other types of ore deposits, and low-grade regional metamorphic rocks. Although much information dealing with the chemical composition, density, and optical properties is available in the literature, many chemical analyses are of questionable accuracy, and no serious attempt has been made to relate the chemical and physical properties for the group as a whole. Few determinations of lattice parameters have been reported, and their variation with composition has not been examined.

With the aid of multiple linear regression analysis, this study examines the relationships between chemical composition and (1) lattice parameters, (2) density, (3) refractive indices, and (4) 2V, for the range of naturally occurring axinites, as represented by 37 specimens from 31 localities (Table 1).

Previous studies

Chemistry and nomenclature

Schaller (1911) examined the available analytical data and recognized the substitutional relationship of Mn and Fe^{2+}, and proposed the end-members *fer-roaxinite*, $Al_2BHCa_2FeSi_4O_{16}$, and *manganoaxinite*,

Table 1. Localities and sources of axinites used in this study

Number	Locality	Source	
1	Val d'Err, near Tinzens, Graubunden, Switzerland	NMNH[1]	95431
2	Obira Mine, Oita-Ken, Kyushu, Japan	NMNH	15210
3	Roscommon Cliff, St. Just, Cornwall, England	NMNH	C6011
4	Le Vernis, Bourg d'Oisans, Isere, France	NMNH	B17121
5	Cassagna Mine, Genova, Italy	NMNH	127774
6	Near Luning, Mineral County, Nevada	NMNH	94407-4
7	Obira Mine, Oita-Ken, Kyushi, Japan	NMNH	R12503
8	McKinney Mine, Mitchell County, North Carolina	NMNH	120244
9	Dauphine, Isere, France	NMNH	R14648
10	Bonsall, San Diego County, California	NMNH	93648
11	Franklin, New Jersey	NMNH	C6233-1
12	Rosebery District, Tasmania, Australia	NMNH	B16838
13	Knappenwand, Tyrol, Austria	NMNH	B17136
14	Mt. Scopi, Mittelrheintal, Switzerland	NMNH	80224
15	Avondale, Delaware County, Pennsylvania	NMNH	87232
16	Kongsberg, Norway	NMNH	B17112
17	Pferdekopf, Wormke, Harz Mountains, Germany	NMNH	B17110
18	Cornog, Pennsylvania	J.A. Speer	
19	Luck Quarry, Shadwell, Virginia	G.R. Lumpkin	
20	Thomaston Dam, Thomaston, Connecticut	C.A. Francis	
21	Feather River, Plumas County, California	J.B. Higgins	
22	Toroku Mine, Miyazaki, Japan	J.B. Higgins	
23	Mineral County, Nevada	J.A. Speer	
24	Saxony, Germany	ANSP[2]	3118
25	Caylloma, Arequipa, Peru	ANSP	20356
26	Dannemora, Sweden	ANSP	23951
27	Tremore, Bodmin, Cornwall, England	ANSP	20104
28	Campbell's Hump, Northampton County, Pennsylvania	ANSP	9282
29	Tremola, Italy	ANSP	3521
30	Kibblehouse Quarry, Perkiomenville, Pennsylvania	ANSP	22210
31	Franklin, New Jersey	NMNH	R3847
32	Franklin, New Jersey	NMNH	C3145
33	Huachuca Mountains, Arizona	NMNH	102822
34	Mt. Scopi, Mittelrheintal, Switzerland	NMNH	B17125
35	Woodlake, California	TM[3]	9620
36	Franklin, New Jersey	NMNH	94946
37	Berg Sroyi, St. Maria, Lukmanier, Switzerland	NMNH	B17127

[1] *Specimens designated NMNH were donated by John S. White of the National Museum of Natural History.*

[2] *Specimens designated ANSP were donated by Robert G. Middleton of the Academy of Natural Sciences of Philadelphia.*

[3] *Specimen TM 9620 was donated by J.J. Finney of the Colorado School of Mines.*

$Al_2BHCa_2MnSi_4O_{16}$. Schaller presumed that the Ca content of axinite was constant.

Now known to be a member of the axinite group, *tinzenite* was originally described as a distinct species by Jakob (1923), who failed to analyze for B_2O_3. The crystallographic and optical similarities of tinzenite and axinite were noted by Parker (1948) and Waldmann (1948), and their isomorphism was finally established by Milton *et al.* (1953), using bulk chemical analyses and X-ray diffraction data. Variability in Ca content of Mn-rich axinites was also noted by Milton *et al.*

Independently, Kurshakova (1968) plotted 78 and Sanero and Gottardi (1968) plotted 17 chemical analyses of axinite on triangular diagrams with vertices Ca–Mn–(Fe+Mg) [Kurshakova (1976) added 26 more analyses]. All compositions plot near one of two lines, either $2Ca \cdot 1(Fe+Mg) \leftrightarrow 2Ca \cdot 1Mn$ or $2Ca \cdot 1Mn \leftrightarrow 1Ca \cdot 2Mn$.

The following nomenclature proposed by Sanero and Gottardi appears adequate to describe the axinites:

(1) *axinite* as the group name.
(2) *ferroaxinite* for Ca > 1.5, Fe > Mn.
(3) *manganaxinite* for Ca > 1.5, Mn > Fe. (called *severingite* by Kurshakova, 1968)
(4) *tinzenite* for Ca < 1.5, Mn > Fe. (called *manganseveringite* by Kurshakova, 1968)

Whether Mn is ordered or disordered in the Ca sites of tinzenite was open to question, so Sanero and Gottardi proposed the general formula $H(Ca,Fe,Mn,Mg)_3Al_2BSi_4O_{16}$ for the axinite group.

Another end-member called *magnesioaxinite* was described by Jobbins *et al.* (1975). This specimen has a composition approaching $HCa_2MgAl_2BSi_4O_{16}$, with no Fe and only 0.4 weight percent MnO. Kurshakova (1976) uses this term for 2Ca-axinites with Mg/(Mg+ Fe) > 0.5, apparently regardless of the Mn content (see her Fig. 9, III). Cassedanne *et al.* (1977) analyzed an iron-rich 2Ca-axinite from Santa Rosa, Bahia, Brazil and found an excess of aluminum (>0.5 atoms per formula unit), which they assigned to the equally under-occupied M^{2+} site. This axinite was deficient in OH, suggesting the charge-balanced substitution $Al^{3+} + O^{2-} \rightleftarrows M^{2+} + OH^-$.

In a study of axinites from Devonshire, England, Chaudry and Howie (1969) found a "reciprocal relationship" between Mg and Mn (but not Fe^{2+} and Mn). In some of their chemical analyses they noted a deficiency of Si with an excess of $Al + Ti + Fe^{3+}$, and they suggested that Al may substitute for Si in tetrahedral coordination. Astakhov *et al.* (1976) examined the ^{57}Fe Mössbauer spectra of an axinite, and found two doublets corresponding to the two oxidation states of iron. They calculated that 5 percent of the iron was Fe^{3+}, and they assumed that it substituted for Al^{3+} in the AlO_5OH octahedra.

Physical properties

Schaller (1911) noted an increase in density of axinite with increasing Mn content, whereas Kurshakova (1968), plotting 3Mn/2(Ca+Mn+Fe+Mg), obtained irregular results. Chaudry and Howie (1969)

could make no correlation between density and composition over the very limited range of their study, but did show a moderate correlation between refractive indices and $(Fe^{3+} + Fe^{2+} + Mn + Ti)$. Gädeke (1938) found a linear variation of mean refractive index with composition for five axinites ranging in composition from 0.33 percent to 12.86 percent MnO; however, Milton *et al.* (1953) noted that tinzenite did not fall on Gädeke's curve, possibly due to low CaO content. Barbour *et al.* (1957) suggest that there is no correlation between $2V$ and the composition of axinite, a conclusion Kurshakova (1968, 1976) appears to support. Kurshakova also notes a linear increase of all three refractive indices with $3Mn/2(Ca+Mn+Fe+Mg)$, but no change in birefringence.

Crystal structure

Peacock (1937) determined the reduced triclinic $P\bar{1}$ cell for axinite, and his paper contains an excellent review of earlier crystallographic studies. He determined lattice parameters by rotation and Weissenberg X-ray techniques and compared them to morphological determinations.

Ito and Takéuchi (1952) first studied the structure of axinite, describing separate Si_4O_{12} rings and BO_3 groups; however, infrared spectra (Plyusina, 1961; Moenke, 1962) and optical absorption spectra (Eremenko, 1971) indicated that boron was in tetrahedral coordination, and Plyusina (1961) suggested that discrete Si_4O_{12} rings did not exist in the structure. Reinvestigation of the structure by Ito *et al.* (1969) and Takéuchi *et al.* (1974) showed the existence of unique $B_2Si_8O_{30}$ groups, in which two boron tetrahedra share three corners each, linking together four Si_2O_7 groups. A nearly rectangular six-membered ring consisting of four silicon- and two boron-containing tetrahedra lies approximately parallel to ($\bar{1}21$) (Takéuchi *et al.*, 1974) and forms the center of each $B_2Si_8O_{30}$ group (Fig. 1a). These $B_2Si_8O_{30}$ groups are nearly planar and are arranged in distinct tetrahedral layers, alternating with sheets of edge-sharing octahedra. The octahedral layers are composed of finite chains of six octahedra of the type Fe–Al–Al–Al–Al–Fe, cross-linked by distorted CaO_6 and $CaO_5(OH)$ polyhedra (Fig. 1b).

Experimental procedures

Electron microprobe analysis

Hand-picked grains of axinite were mounted in epoxy, polished, and carbon-coated for analysis using a nine-spectrometer ARL-SEMQ microprobe operated

at 15 kV, 100 nA. Elements analyzed for included Ti, Na, and K (these were not detected at the 0.05 weight percent level), Zn (found only in specimens from Franklin, New Jersey), and the major elements Ca, Fe, Mg, Mn, Al, B, and Si. A chemically-analyzed axinite (Bourg d'Oisans, France, 6.12 weight percent B_2O_3) was used as a boron standard, but count rates were extremely low (6–7 cps above background). For that reason boron was ultimately assumed to be stoichiometric, as was OH. Data reduction was accomplished using the program MAGIC IV by John Colby, adapted for the ARL-SEMQ by William Hamilton.

Density

Specimens weighing between 15 and 25 mg were hand-picked under a microscope for density measurements, using a Berman balance with toluene as the buoyant medium. Each density reported is the mean of five determinations, each corrected for temperature.

Lattice parameters

Lattice parameters of 10 axinites were determined from X-ray powder patterns with BaF_2 as an internal standard. The BaF_2 [$a = 6.198(2)$Å] was annealed five times for two hours each at 800°C (J. A. Speer, personal communication). The powder patterns were run on a Picker diffractometer with monochromatized CuKα radiation, 1 inch/min chart speed, 0.5° 2θ/min scan rate, and a 1° receiving slit. Ambiguity in indexing was overcome by reference to calculated powder patterns for each of the four axinite end-members based on the structure refinement of Takéuchi *et al.* (1974). The least-squares program of Appleman and Evans (1973) was used to refine the lattice parameters with starting parameters taken from Takéuchi *et al.* (1974).

Optical properties

Refractive indices and the optic axial angle $2V$ were determined by the spindle stage technique of Bloss (in press). Using the computer program of Bloss and Riess (1973), we calculated optic axial angle and spindle stage coordinates for the measurement of refractive indices from extinction data taken in sodium light. For each principal vibration direction the wavelength of match was recorded in at least five refractive index oils. The index of match was then corrected for temperature, and the data were fitted to a linearized Sellmeier equation from which the refractive indices were calculated for sodium light. The
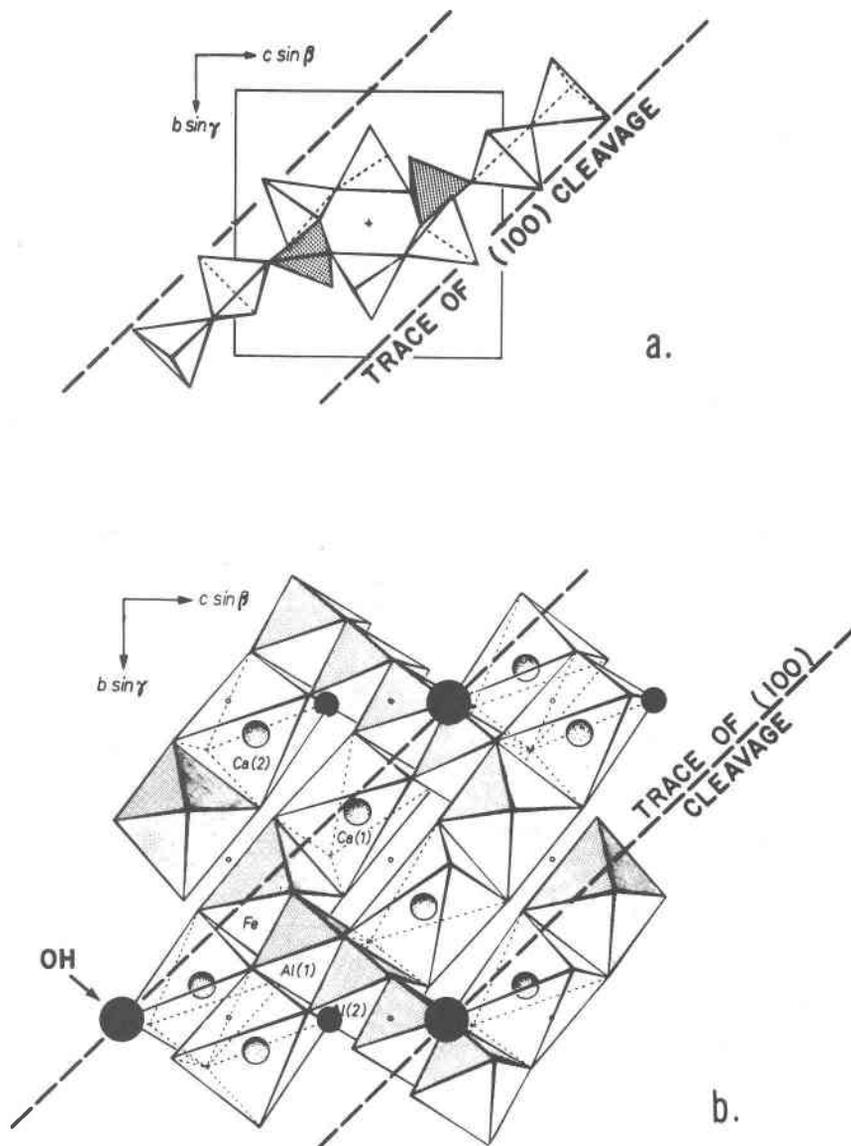
Fig. 1. Projections down the a axis of the axinite structure. (a) Tetrahedral layer: the $B_2Si_8O_{30}$ group with {100} cleavage traces shown as dashed lines. (b) The octahedral layer: large dots are OH ions in the upper anion layer, smaller dots are OH ions in the lower layer. OH ions lie on the {100} cleavage traces. The (100) plane is inclined ~14° to the plane of the drawing. Figures modified from Takéuchi *et al*. (1974).

maximum estimated error for refractive indices is ±0.001. The orientation of the biaxial indicatrix relative to the crystallographic directions (Fig. 5) was obtained for a manganaxinite from Franklin, New Jersey (sample no. 11) by alignment of the crystal on an X-ray precession camera subsequent to its characterization on the spindle stage.

Chemical analyses, lattice parameters, densities, refractive indices, and $2V$ are compiled in Tables 2 and 3.

Discussion of results

Chemistry

The range in composition of axinites is represented by substitutional solid solution among the divalent, octahedrally-coordinated cations Ca, Mn, Fe, Mg, and Zn, which can best be seen on two triangular diagrams. Figure 2 has vertices 3Ca–3Mn–3(Fe+ Mg+Zn). It includes all known axinite compositions (see Tables 2 and 3), and substantiates the con-

Table 2. Microprobe analyses, refractive indices, $2V\alpha$, density, and lattice parameters for 14 axinites

Specimen	1	5	6	7	8	11	12	15	17	19	33	(35)	(1)	(3)
CaO (wt %)	12.01	13.77	20.15	19.00	19.71	18.59	19.18	19.27	20.12	19.71	18.76	19.59	21.7	20.1
MnO	20.74	18.57	3.35	5.83	9.48	12.36	2.61	9.55	1.23	3.23	12.39	6.59	0.4	3.3
FeO	2.48	0.55	4.32	6.44	2.85	1.88	10.41	3.41	7.94	7.83	1.10	5.21	n.d.	8.1
MgO	0.20	0.17	3.03	0.76	0.40	0.13	0.66	0.21	2.20	1.20	0.53	0.62	6.9	1.6
ZnO	n.d.	n.d.	n.d.	n.d.	n.d.	1.43	n.d.	n.d.	n.d.	n.d.	n.d.	n.d.	0.06	n.d.
Al_2O_3	15.41	17.95	18.52	18.63	17.27	16.61	17.24	17.80	18.21	17.96	17.45	17.83	17.9	17.5
$(B_2O_3)*$	(6.00)	(6.04)	(6.26)	(6.14)	(6.11)	(6.10)	(6.14)	(6.12)	(6.21)	(6.16)	(6.12)	(6.13)	--	--
SiO_2	41.22	41.41	42.72	41.09	41.55	41.44	41.97	42.59	42.80	42.55	41.80	41.86	44.0	42.2
$(H_2O)*$	(1.53)	(1.56)	(1.61)	(1.57)	(1.56)	(1.56)	(1.57)	(1.59)	(1.61)	(1.59)	(1.57)	(1.57)	--	--
Sum	99.59	100.02	99.96	99.46	98.93	100.10	99.78	100.54	100.32	100.23	99.72	99.40	--	--
TM**	0.655	0.578	0.249	0.383		0.456	0.396	0.400	0.291	0.346	0.412		0.021	
α	1.694	1.691	1.669	1.683		1.685	1.682	1.682	1.674	1.677	1.683		1.656	1.672
β	1.700	1.697	1.675	1.691		1.692	1.690	1.689	1.682	1.684	1.689		1.660	1.679
γ	1.705	1.701	1.680	1.694		1.695	1.693	1.692	1.685	1.687	1.693		1.668	1.682
$2V_\alpha$ (°)	87.8(2)	77.1(3)	80.4(1)	69.6(3)	64.5(6)	75.7(2)	67.7(2)	60.7(4)	73.2(4)	67.8(3)	77.4(3)			

clusions of Sanero and Gottardi (1968) that the major substitutions fall on either of two lines: $2Ca \cdot 1(Fe+Mg) \leftrightarrow 2Ca \cdot 1Mn$ or $2Ca \cdot 1Mn \leftrightarrow 1Ca \cdot 2Mn$.

The substitution of Mn for Ca in the distorted Ca1 and Ca2 sites (Fig. 1b) is represented by the numbered specimens in Figure 2: 1, 5, *11*, 25, *31*, *32*, 33, and *36* (those in italics contain zinc). The remainder of the analyses, shown as unnumbered points, plot near the line where Ca $\approx$ 2.00 atoms per formula unit, and they can best be described separately on a triangular diagram with vertices Mn–Fe–Mg (Fig. 3). This diagram illustrates substitutional relationships in the Fe site (Fig. 1b) and also shows the variation of $2V\alpha$ with composition for the 2Ca-axinites.

Silicon was found to be stoichiometric (4.00 atoms per formula unit) within ±1 percent of the amount present for 36 of 37 analyses. The exception is speci-

Table 2. (continued)

Specimen	1	5	6	7	8	11	12	15	17	19	(35)	(1)	(3)
ρ_{obs} (g/cc)	3.393(10)	3.403(10)	3.249(6)	3.314(7)	3.300(6)	3.328(10)	3.281(1)	3.318(3)	3.253(6)	3.275(4)	3.290(5)	3.178	3.288
ρ_{calc} (g/cc)	3.426	3.387	3.255	3.308	3.313	3.357	3.325	3.312	3.278	3.300	3.309	3.202	
<r>***	0.764	0.759	0.768	0.771	0.778	0.777	0.771	0.775	0.767	0.770			
a (Å)	7.158(6)	7.153(5)	7.156(2)	7.156(2)	7.162(4)	7.161(4)	7.157(1)	7.160(2)	7.153(1)	7.159(2)	7.157(2)	8.933	8.953
b (Å)	9.184(11)	9.169(8)	9.193(3)	9.203(2)	9.208(6)	9.213(6)	9.201(2)	9.209(3)	9.191(4)	9.195(4)	9.200(2)	9.155	9.197
c (Å)	8.958(5)	8.945(7)	8.955(4)	8.960(2)	8.972(6)	8.974(6)	8.962(2)	8.965(3)	8.957(4)	8.958(3)	8.959(2)	7.121	7.143
α (°)	91.97(10)	91.86(6)	91.85(3)	91.83(3)	91.87(4)	91.80(6)	91.85(2)	91.85(3)	91.83(2)	91.83(3)	91.8(8)	102.59	102.63
β (°)	98.31(12)	98.40(6)	98.08(3)	98.08(2)	98.09(7)	98.11(5)	98.15(2)	98.07(3)	98.12(2)	98.09(3)	98.14(2)	98.28	98.10
γ (°)	77.29(8)	77.16(7)	77.35(3)	77.29(2)	77.29(6)	77.24(5)	77.31(1)	77.30(2)	77.33(2)	77.29(3)	77.30(2)	88.09	88.21
Vol (Å³)	568.5(7)	565.8(5)	569.1(3)	570.0(2)	571.4(4)	571.7(4)	569.9(2)	571.0(2)	568.8(1)	569.5(3)	569.8(2)	562.4	568.2

n.d. = not detected. (35) Lattice parameters from Takeuchi et al. (1974). (1) and (3) are from Jobbins et al. (1975)

*B_2O_3 contents were interpolated from curves prepared for pure end-members, H_2O was calculated using the computer program SUPER RECAL of J. C. Rucklidge (personal communication).

**TM = $\dfrac{\text{wt. \% (MnO + FeO + ZnO)}}{\text{wt. \% (MnO + FeO + ZnO + CaO+MgO)}}$

*** <r> = mean radius of octahedral cations

Table 3. Microprobe analyses, $2V\alpha$, and density for 25 axinites

Specimen	2	3	4	9	10	13	14	16	18	20	21	22	23
CaO (wt.%)	19.65	19.49	19.76	19.70	19.64	19.94	19.88	19.88	19.62	20.01	20.01	19.70	19.87
MnO	5.66	3.42	2.05	3.35	1.56	2.82	2.17	3.98	4.84	1.32	0.98	2.52	4.87
FeO	4.93	9.32	8.52	6.36	8.52	7.67	8.40	6.70	6.57	8.03	7.53	9.58	6.03
MgO	1.49	0.63	1.49	1.89	1.85	1.44	1.43	1.34	0.79	2.07	2.55	0.73	1.31
ZnO	n.d.	n.d.	n.d.	n.d.	n.d.	n.d.	n.d.	n.d.	n.d.	n.d.	n.d.	n.d.	n.d.
Al_2O_3	17.91	17.14	17.84	18.35	18.34	17.94	18.08	18.01	17.91	18.23	18.23	17.56	17.69
(B_2O_3)*	(6.18)	(6.12)	(6.16)	(6.20)	(6.19)	(6.17)	(6.17)	(6.17)	(6.14)	(6.21)	(6.22)	(6.13)	(6.17)
SiO_2	42.22	41.59	41.88	42.54	42.42	42.03	42.45	42.61	42.25	42.52	42.74	41.83	42.12
(H_2O)*	(1.59)	(1.56)	(1.58)	(1.60)	(1.60)	(1.59)	(1.60)	(1.60)	(1.58)	(1.60)	(1.61)	(1.57)	(1.58)
Sum	99.63	99.27	99.28	99.99	100.12	99.60	100.18	100.29	99.70	99.99	99.87	99.62	99.64
TM**	0.334	0.388	0.332	0.310	0.319	0.329	0.332	0.335	0.359	0.297	0.274	0.372	0.340
$2V_\alpha$ (°)	74.2(7)	68.7(3)	72.0(3)	73.1(1)	73.1(2)	71.4(3)	70.5(5)	72.7(4)	67.8(3)		74.0(1)	67.8(2)	70.5(4)
ρ_{obs} (g/cc)	3.295(7)	3.315(8)	3.292(9)	3.269(5)	3.276(6)	3.295(7)	3.287(5)	3.274(5)	3.290(5)	3.273(6)	3.231(8)	3.298(9)	3.278(6)

n.d. = not detected; *, ** see footnotes in Table 2.

men 7 from Obira, Japan, in which a deficiency of 0.089 atoms per formula unit is almost exactly balanced by an excess of 0.090 Al atoms, suggesting a substitution of Al for Si in tetrahedral coordination [*cf.* Chaudry and Howie (1969), who suggest a similar substitution in axinites from Devonshire, England].

Except for specimen 7 with 4.5 percent excess aluminum, presumably in tetrahedral coordination, aluminum was found to be stoichiometric (2.00 atoms per formula unit) within ±2 percent of the amount present for 30 of the 37 analyses. Specimen 1

from Tinzens, Switzerland, contains the least aluminum (1.78 atoms per formula unit) but shows an excess 1.22 (Mn+Fe+Mg) normally assigned to the single Fe site. It is presumed that all of the iron (0.20 atoms) in this specimen is Fe^{3+} and that it substitutes for Al^{3+} in the Al1 and Al2 octahedral sites (see Fig. 1b). Specimen 11 from Franklin, New Jersey contains 1.88 Al and 1.19 (Mn+Fe+Mg)—a slight excess of total cations for the three octahedral sites, but sufficient iron as Fe^{3+} to compensate for "missing" Al in the Al1 and Al2 sites. Similar assumptions can be

Table 3. (continued)

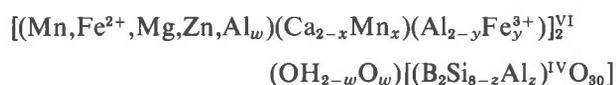| Specimen	24	25	26	27	28	29	30	31	32	34	36	37
CaO	19.80	19.05	19.12	19.94	19.77	19.78	19.38	18.00	19.25	19.81	18.30	19.76
MnO	3.83	12.33	9.23	3.98	6.20	2.40	5.67	12.74	11.79	1.09	11.79	2.28
FeO	7.95	1.21	3.06	8.41	3.68	7.50	5.99	0.99	0.73	8.76	1.18	8.33
MgO	0.69	0.21	0.49	0.30	1.69	1.73	0.98	0.14	0.14	1.87	0.13	1.53
ZnO	n.d.	n.d.	n.d.	n.d.	n.d.	n.d.	n.d.	2.23	1.80	n.d.	2.20	n.d.
Al_2O_3	18.01	17.47	18.11	17.56	18.23	18.02	17.96	17.30	17.67	17.89	17.38	17.78
(B_2O_3)*	(6.14)	(6.12)	(6.13)	(6.12)	(6.19)	(6.17)	(6.15)	(6.11)	(6.12)	(6.18)	(6.10)	(6.17)
SiO_2	42.44	42.06	41.80	41.98	42.17	41.82	41.84	41.60	42.06	42.12	41.55	42.09
(H_2O)*	(1.59)	(1.58)	(1.58)	(1.58)	(1.59)	(1.58)	(1.58)	(1.58)	(1.57)	(1.59)	(1.57)	(1.58)
Sum	100.45	100.03	99.52	99.87	99.52	99.00	99.55	100.68	101.12	99.31	100.20	99.52
ρ_{obs} (g/cc)						3.272(3)	3.290(3)					
$2V_\alpha$ (°)	67.3(1)	72.5(1)			74.5(4)		71.6(4)	74.1(4)			74.6(4)	
TM	0.365	0.413	0.385	0.380	0.315	0.315	0.362	0.468	0.425	0.312	0.451	0.333
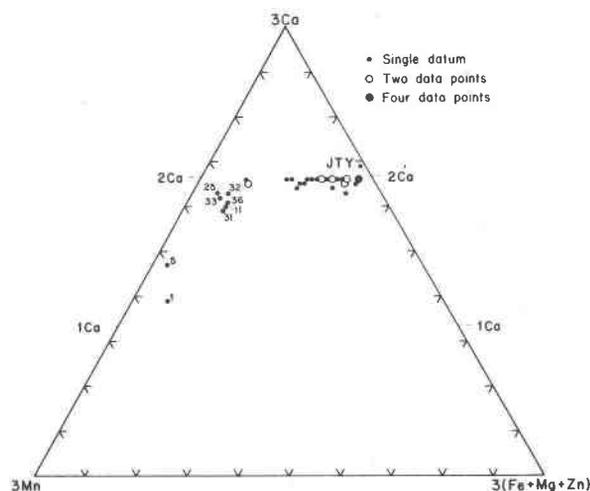
Fig. 2. Triangular diagram similar to that devised by Sanero and Gottardi (1968) (cf. Kurshakova, 1968) to display the compositional range of the axinites. The unnumbered specimens are also plotted in Fig. 3 on an Mn–Fe–Mg diagram. The numbered specimens contain less than 2 Ca atoms. The data for the point labeled JTY is taken from Jobbins et al. (1975).

Fig. 3. Triangular diagram showing the Mn–Fe–Mg contents [normalized to (Mn+Fe+Mg) = 1.00] of 2Ca-axinites. The magnesioaxinite of Jobbins et al. (1975) is included on the plot, and its $2V\alpha$ value, calculated from refractive indices, is shown. This diagram has been partially contoured for $2V\alpha$ using data from Tables 2 and 3.

made concerning specimens 3, 8, 12 and 36, which contain between 1.93 and 1.95 Al atoms and sufficient excess (Mn+Fe+Mg) to allow for a partitioning of Fe^{3+} into the Al sites.

Specimens 11, 31, 32 and 36 from the Fe–Mn–Zn deposits of Franklin, New Jersey are the only axinites containing significant amounts of zinc (1.43–2.23 weight percent). They occur in hydrothermal veins and as products of hydrothermal alteration of calc-silicates (Frondel and Baum, 1974).

Structural formula

Based on the structure refinement of Takéuchi et al. (1974) and this and previous chemical investigations, a new structural formula is proposed for axinite:

$$[(Mn,Fe^{2+},Mg,Zn,Al_w)(Ca_{2-x}Mn_x)(Al_{2-y}Fe_y^{3+})]_2^{VI}$$

$$(OH_{2-w}O_w)[(B_2Si_{8-z}Al_z)^{IV}O_{30}]$$

where $w < 1$, $x < 1$, $y \ll 1$, $z \ll 1$, and VI and IV represent the coordination numbers of the cations.

Density

Multiple linear regression analysis of densities considered together with a number of compositional variables (such as mole fraction transition metals and mole and weight fraction of individual elements) led to the selection, on the basis of highest F ratios and
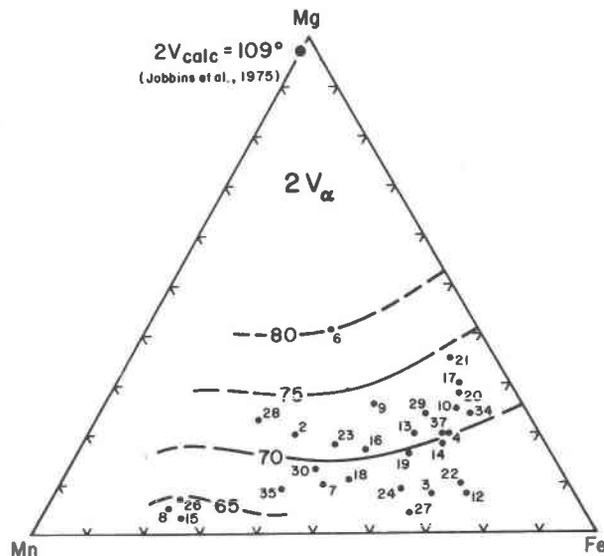
$|t|$ tests, of the ratio TM (for Transition Metals) ≡ weight percent (MnO+FeO+ZnO)/weight percent (MnO+FeO+ZnO+CaO+MgO) as the variable most highly correlated to the observed density. Data
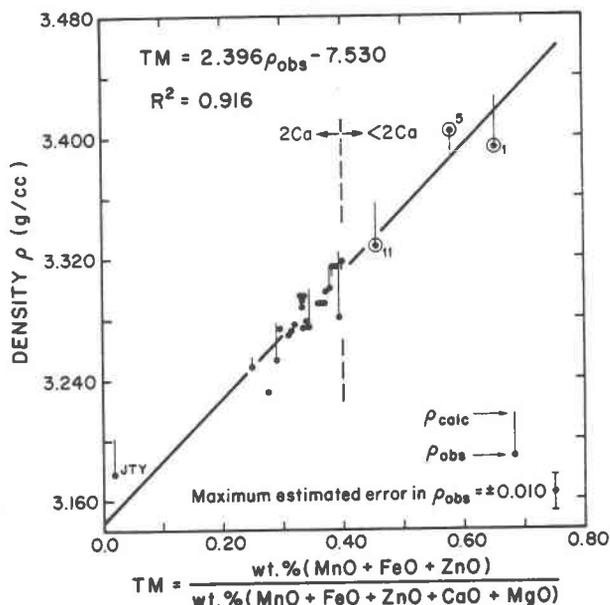

Fig. 4. Plot of density vs. TM for 27 axinites. Calculated densities for those specimens whose lattice parameters were known (Table 2) are indicated by the end of the vertical line extending from the ρ_{obs} data points. JTY refers to the density reported by Jobbins et al. (1975) for magnesioaxinite. Specimens with less than 2 Ca atoms per formula unit are circled and numbered.
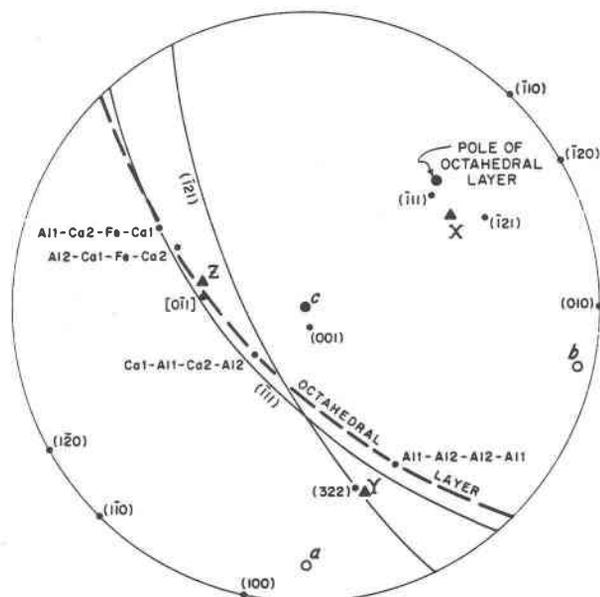
Fig. 5. Stereographic projection showing the orientation of the biaxial indicatrix (triangles labelled X, Y, Z) relative to the crystallographic directions (a,b,c) for specimen 11. Also plotted are poles of the major structural features in axinite, notably the octahedral chains labeled with the sequence of sites encountered along them. The octahedral layer (heavy dashed line), which includes all four octahedral chains, is very nearly parallel to ($\overline{1}11$).

are shown in Figure 4, and the equation is

$$TM = 2.396\rho_{obs} - 7.530$$

The correlation coefficient $R^2 = 0.916$. The 2Ca-axinites plot with TM values of less than 0.40, whereas axinites with TM values greater than 0.40 have less than 2 Ca atoms per formula unit.

Forms and cleavage

Figure 5 is a stereographic projection in which the vectors joining the ends of the Al1–Al2–Al2–Al1, Al1–Ca2–Fe–Ca1, Al2–Ca1–Fe–Ca2, and Ca1–Al1–Ca2–Al2 octahedral chains are plotted. They all lie on a great circle approximately parallel to the ($\overline{1}11$) plane in axinite, and it is presumed that the orientation of the octahedral layer is well defined by these chains. The tetrahedral ring, near ($\overline{1}21$) (Takéuchi *et al.*, 1974), is nearly parallel to the octahedral layer. The structural influence of this pronounced layering on external morphology is indicated by a clustering of ($\overline{h}kl$) and ($\overline{h}k0$) face poles near the face pole of the octahedral layer (*cf.* Fig. 1 in Peacock, 1937). The planes represented by these face poles generally lie at an angle of 30° or less to the plane of the octahedral layer. Axinite crystals are frequently flattened by

some combination of the forms {010}, {011}, {$\overline{1}11$}, {$\overline{1}21$}, {$\overline{1}10$}, and {$\overline{1}20$}.

The {100} cleavage in axinite results from a distinct banding of the $B_2Si_8O_{30}$ groups parallel to [$0\overline{1}1$] in the tetrahedral layer. The dashed lines in Figure 1a show the trace of the {100} cleavage parallel to the elongated $B_2Si_8O_{30}$ group. The cleavage plane is inclined at ~14° to the plane of the figure. The trace of {100} in the octahedral layer is seen in Figure 1b. Notice that it runs through the hydroxyl groups bonded to Ca2 and both Al1 and Al2. Thus, by cleaving on {100}, the integrity of the tetrahedral bands are preserved and only weak (Ca,Al)–(OH,O) and (Fe,Mn,Mg)–O bonds need be broken in the octahedral layer.

Optical properties

The variation of mean refractive index was also shown by multiple linear regression analysis to be best described in terms of the variable TM, and the following equation relating composition to mean refractive index ⟨R.I.⟩ was determined for the data plotted in Figure 6:

$$TM = 15.475\langle R.I.\rangle - 25.700 \qquad (R^2 = 0.965)$$

A dashed vertical line at $TM = 0.40$ again serves as a boundary between the 2Ca-axinites and axinites with less than two Ca atoms per formula unit. Since all data points fall within two standard deviations of the line defined by this equation, a second-order curve was not fitted to the data; however, it may be possible to describe the variation in mean refractive index
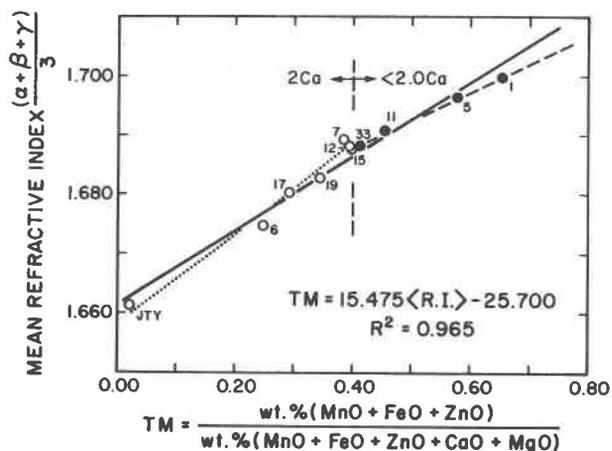

Fig. 6. Plot of mean refractive index *vs. TM*. The regression equation refers to the solid line for all data points. The filled circles and dashed line are for axinites with less than 2.0 Ca atoms and the open circles and dotted line are for 2Ca-axinites (refer to text for regression equations).

with composition by two line segments, one for the 2Ca-axinites defined by the equation:

$$TM = 13.323 \langle R.I. \rangle - 22.093 \quad (R^2 = 0.975)$$

and one for axinites with less than 2 Ca atoms per formula unit defined by the equation:

$$TM = 21.443 \langle R.I. \rangle - 35.784 \quad (R^2 = 0.999)$$

As mentioned earlier, Figure 3 was partially contoured to show the variation of the optic axial angle with composition for the zinc-free 2Ca-axinites. It indicates an increase in $2V\alpha$ with increasing Mg content. This is probably the result of Mg entering the Fe sites which are located on the ends of the Al1–Al2–Al2–Al1 octahedral chains (Fig. 1b) and oriented nearly parallel to Y, the principal vibration direction for the β refractive index (Fig. 5). As Mg substitution increases, β decreases at a faster rate than α and γ, causing an increase in $2V\alpha$ and eventually a change in optic sign from negative to positive, as shown by the magnesioaxinite of Jobbins et al. (1975). The $2V\alpha$ value calculated from refractive indices for this nearly pure magnesian end-member is 109°.

The orientation of the biaxial indicatrix in relation to the crystallographic directions and structural features of axinite is presented in Figure 5 for specimen 11. The Z principal vibration direction is oriented nearly parallel to [0$\bar{1}$1], which is the direction of elongation of the $B_2Si_8O_{30}$ groups (cf. Fig. 1a), and plots among the poles representing the directions of the three Ca-containing octahedral chains. As mentioned earlier, Y is oriented near the Al1–Al2–Al2–Al1 octahedral chains which are terminated at each end with Fe-octahedra (cf. Fig. 1b), and X is at an angle of ~79° to the octahedral layer and ~80° to the ($\bar{1}$21) plane of the tetrahedral $B_2Si_4O_{12}$ ring. This indicatrix orientation is similar to that found in the optically-negative micas, where Z and Y lie parallel or nearly parallel to the plane of the tetrahedral and octahedral layers and X is normal or nearly normal to the plane of layering.

Lattice parameters

The lattice parameters of each of 10 axinites were determined from 30 to 40 powder diffraction peaks in the range 9–70°2θ; they are recorded in Table 2. The cell edges a, b, and c are plotted in Figure 7 as a function of $\langle r \rangle$, the mean radius of cations occupying the Ca1, Ca2, Fe, Al1 and Al2 octahedral sites. Their variation can best be discussed with reference to the stereonet in Figure 5. Unfortunately the reduced triclinic cell of axinite leaves none of the axial zones
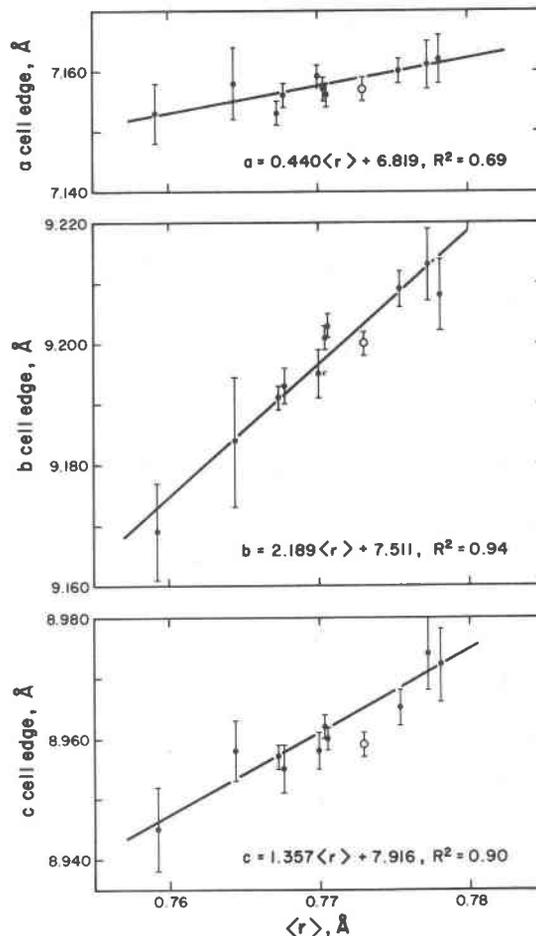

Fig. 7. Lattice parameters a, b, and c of the axinites listed in Table 2, plotted vs. $\langle r \rangle$, the mean radius of cations occupying the Ca1, Ca2, Fe, Al1 and Al2 octahedral sites. Error bars are shown for each datum, and the cell edges of Takéuchi et al. (1974), which were not used in the regression, are included for comparison (open circles). The lattice parameters determined by Jobbins et al. (1975) and listed in Table 2 fall significantly below these curves; they were not plotted because the authors gave no indication of the use of an internal standard.

oriented along major structural features. The zone [0$\bar{1}$1] comes closest to the octahedral chains Al1–Ca2–Fe–Ca1, Al2–Ca1–Fe–Ca2, and Ca1–Al1–Ca2–Al2, among which the primary cation substitutions occur. Thus it is not surprising that the linear regression equations for b (inclined at 32° to chain Al1--- and at 36° to chain Al2---), for c (inclined at 50 and 58° to Al1--- and Al2--- and at 26° to chain Ca1---), and for a (inclined at high angles to all these octahedral chains) have slopes in the ratio 5:3:1 and coefficients of correlation $R^2 = 0.94$, 0.90, and 0.69. As anticipated, the unit-cell volume is most highly correlated with $\langle r \rangle^3$ (see Fig. 8).
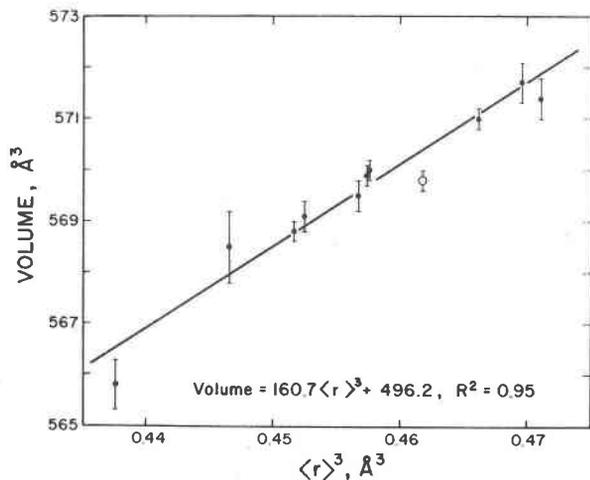
Fig. 8. Plot of the unit-cell volume of axinite *vs.* the cube of the mean radius of cations occupying the Ca1, Ca2, Fe, Al1 and Al2 sites. The datum of Takéuchi *et al.* (1974) is plotted as an open circle for purposes of comparison.
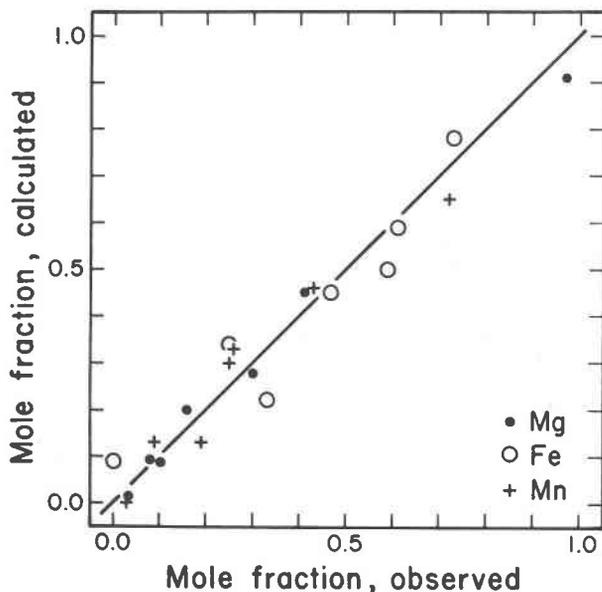

Fig. 9. Combined plot of the observed mole fractions of Mg, Fe, and Mn for seven axinites *vs.* the values calculated from the multiple regression equations given in the text. Both observed and calculated values were normalized to $(Mg+Fe+Mn) = 1.00$ before plotting, because totals ranged between 0.95 and 1.05. The line has a slope of 45°.

Composition of 2Ca-axinites from optical properties and density

Mean refractive index, $2V\alpha$, and density for 7 non-zincian 2Ca-axinites were used to determine multiple linear regression equations for the individual calculations of the mole fractions of Mg, Fe, and Mn by the Biomedical Computer Program BMDO3R (Dixon, 1973). The results are tabulated below; standard errors of regression coefficients are listed in parentheses below the coefficient.

$$Mg = -14.333\langle R.I.\rangle + 0.012(2V\alpha) + 23.487$$
$$\quad\quad (3.268) \quad\quad\quad (0.002)$$
$$(R^2 = 0.997)$$

$$Fe = 71.937\langle R.I.\rangle - 11.810(\rho_{obs}) - 81.890$$
$$\quad\quad (14.547) \quad\quad (3.042)$$
$$(R^2 = 0.894)$$

$$Mn = -42.903\langle R.I.\rangle + 12.523(\rho_{obs}) + 31.473$$
$$\quad\quad (12.445) \quad\quad (2.602)$$
$$(R^2 = 0.910)$$

The pair of variables in each equation is the combination having the greatest statistical significance. Inclusion of ρ_{obs} in the equation for Mg resulted in a decrease in the F-ratio from 577 to 311 and a $|t|$ value for ρ_{obs} of 0.197, which may be rejected at the 20 percent confidence level. Inclusion of $2V\alpha$ in the equations for Fe and Mn results in decreased F-ratios and $|t|$ values of 0.960 and 0.380 respectively, which can be rejected as being significant at the 60 percent

and 30 percent confidence levels, respectively. A plot of calculated *vs.* observed Mg, Fe, and Mn mole fractions (Fig. 9) suggests that the above equations provide a reasonable estimate of composition for the non-zincian 2Ca-axinites. However, better correlations based on identical variables should result for the three equations upon acquisition of additional data for multiple regression analysis.

The $2V\alpha$ values for the numbered specimens in Figure 2 do not fit the pattern of the non-zincian 2Ca-axinites (unnumbered in Fig. 2) plotted in Figure 3. The zinc-bearing Franklin, New Jersey specimens (11, 31, 36) have $2V$ values of 75.7°, 74.1°, and 74.6°, respectively. Specimens 25 and 33 with nearly the same composition (Tables 2 and 3) have $2V\alpha = 72.5°$ and 77.4°, and specimen 5 with 1.42 Ca and specimen 1 with 1.26 Ca have $2V$ values of 77.1° and 87.8°, respectively. Clearly additional study is required to complete the optical characterization of the axinites, especially those with less than two Ca atoms per formula unit.

References

Appleman, D. E. and H. T. Evans, Jr. (1973) Job 9214: Indexing and least-squares refinement of powder diffraction data. *Natl. Tech. Inf. Serv., U.S. Dept. Commerce, Springfield, Virginia, Document PB-216 188.*

Astakhov, A. V., Yu. B. Voitkovskii, O. N. Generalov and S. V. Sidorov (1976) NGR investigation of some lamellar and boron-containing silicates. *Sov. Phys. Crystallogr., 20,* 471–474.

Barbour, E. A., H. H. Bird and D. P. Gold (1957) An occurrence of axinite in Ventersdorp lavas from Kinross, Transvaal, South Africa. *Mineral. Mag., 31,* 495–496.

Bloss, F. D. (in press) *The Spindle Stage: Principles and Practice.* Cambridge University Press, Cambridge, England.

——— and D. Riess (1973) Computer determination of $2V$ and indicatrix orientation from extinction data. *Am. Mineral., 58,* 1052–1061.

Cassedanne, J., J. Cassedanne and N. Estrada (1977) Le gîte d'axinite de Santa Rosa (municipe de Condeúba, État de Bahia, Brésil). *Bull. Soc. fr. Mineral. Cristallogr., 100,* 191–197.

Chaudry, M. N. and R. A. Howie (1969) Axinites from the contact skarns of the Meldon aplite, Devonshire, England. *Mineral. Mag., 37,* 45–48.

Dixon, W. J. (Ed.) (1973) *BMD, Biomedical Computer Programs.* University of California Press, Berkeley, California.

Eremenko, G. K. (1971) Optical absorption spectra of axinite group minerals. *Dopov. Akad. Nauk Ukr.SSR, Ser. B 33(9),* 783–788.

Frondel, C. and J. L. Baum (1974) Structure and mineralogy of the Franklin zinc-iron-manganese deposit, New Jersey. *Econ. Geol., 69,* 157–181.

Gädeke, R. (1938) Die Gesetzmässigen Zusammenhänge und Anomalien in der Vesuviangruppe und einigen anderen Kalksilikaten. *Chem. Erde, 11,* 592–636.

Ito, T. and Y. Takéuchi (1952) The crystal structure of axinite. *Acta Crystallogr., 5,* 202–208.

———, ———, T. Ozawa, T. Araki, T. Zoltai and J. J. Finney (1969) The crystal structure of axinite revised. *Proc. Japan Acad., 45,* 490–494.

Jakob, J. (1923) Vier Mangansilikate aus den Val D'Err (Kanton Graubünden). *Schweiz. Mineral. Petrogr. Mitt., 3,* 227–236.

Jobbins, E. A., A. E. Tresham and B. R. Young (1975) Magnesioaxinite, new mineral found as a blue gemstone from Tanzania. *J. Gemmol., 14,* 368–375.

Kurshakova, L. D. (1968) *Metasomatism and Other Physical-Chemical Processes in Petrology,* p. 289–311. Publishing House Nauka, Moscow.

——— (1976) *Physical-Chemical Conditions of Formation of Skarn Borosilicate Deposits.* Publishing House Nauka, Moscow.

Milton, C., F. A. Hildebrand and A. M. Sherwood (1953) The identity of tinzenite with manganoan axinite. *Am. Mineral., 38,* 1148–1158.

Moenke, H. (1962) Fortschritte auf dem Gebiet der Ultrarotspektroscopie II. Nachweis von BO_3- und BO_4-Gruppen in den haufigsten naturlich gebildeten Silikaten. *Silikat.-Techn., 13,* 287–288.

Parker, R. L. (1948) Zur Kristallographie von Tinzenit. *Schweiz. Mineral. Petrogr. Mitt., 28,* 475–492.

Peacock, M. A. (1937) On the crystallography of axinite and the normal setting of triclinic crystals. *Am. Mineral., 22,* 588–624.

Plyusina, I. I. (1961) Infrared spectra of ring silicates, III. *Zh. Strukt. Khim., 2,* 330–336.

Sanero, E. and G. Gottardi (1968) Nomenclature and crystal chemistry of axinites. *Am. Mineral., 53,* 1407–1411.

Schaller, W. T. (1911) Mineralogical notes, Series I, Axinite from California. *U.S. Geol. Surv. Bull. 490.*

Takéuchi, Y., T. Ozawa, T. Ito, T. Araki, T. Zoltai and J. J. Finney (1974) The $B_2Si_8O_{30}$ groups of tetrahedra in axinite and comments on the deformation of Si tetrahedra in silicates. *Z. Kristallogr., 140,* 289–312.

Waldmann, H. (1948) Über die Kristalloptik von Tinzenit. *Schweiz. Mineral. Petrogr. Mitt., 28,* 493–501.